IEEE Access
Multidisciplinary | Rapid Review | Open Access Journal

Received June 13, 2018, accepted July 9, 2018, date of publication July 17, 2018, date of current version September 5, 2018.

Digital Object Identifier 10.1109/ACCESS.2018.2856806

An Extraction and Classification Algorithm for Concrete Cracks Based on Machine Vision

SUN LIANG[1], XING JIANCHUN[1], AND ZHANG XUN[2]
[1]College of Defense Engineering, PLA University of Science and Technology, Nanjing 210007, China
[2]High-tech Institute, Qingzhou 262500, China

Corresponding author: Sun Liang (sunyaoyuazly@163.com)

This work was supported in part by the National Natural Science Foundation of China under Grant 61602507 and in part by the Natural Science Foundation of Jiangsu Province of China under Grant BK20150723.

ABSTRACT To solve the problem of large errors in extraction and the difficulty in classifying crack images in health monitoring of civil engineering structures, a new classification algorithm of concrete crack extraction based on machine vision is proposed in this paper. First, the gray difference between the image and the background is expanded by an adaptive nonlinear grayscale transformation. The improved OTSU threshold segmentation is used to extract the cracks, and the fracture points in the extracted results are connected by combining the extension direction of the fracture skeleton line and the gray feature of the crack edge to obtain the complete crack image. At the same time, the number of bifurcation points of the fracture skeleton line is calculated, a gray projection histogram of X axis and Y axis is obtained. Then, the classification characteristics of the cracks, such as the peak ratio of the gray histogram, the distribution ratio of the projection interval, and the mean square deviation ratio of the gray histogram are calculated. The obtained features are used as input to train a support vector machine classifier, which is then used to perform crack classification. The results of a simulation show that the proposed algorithm can extract crack images completely and precisely and can quickly and accurately classify the various types of cracks; thus, it has a good detection ability.

INDEX TERMS Crack image, nonlinear grayscale transformation, gray projection, mean square error, support vector machine.

I. INTRODUCTION

Scientific and technological advances have resulted in the development and construction of a series of new civil engineering structures such as port wharfs, cross-sea bridges and undersea tunnels [1] that greatly facilitate people's daily lives. However, most civil engineering structures in harsh natural environment are prone to corrosion and damage from natural factors such as seawater, wind, ice and fog [2]. Therefore, conducting structural health monitoring for these structures is highly important. Cracks are the most direct and most common manifestation of civil engineering structure damage; thus, the key to structural health monitoring of civil engineering structures is to achieve effective methods for monitoring and treating cracks [3]. Using artificial and traditional methods to monitor cracks is not only time consuming and labor intensive but also makes achieving the desired accuracy difficult [4]. Instead, adopting video surveillance to monitor ocean engineering structures, in combination with machine vision algorithms to process the video images and extract the key geometric information of the crack is both a more accurate and more practical approach.

To effectively extract and classify crack images, scholars have conducted extensive research. Long *et al.* [5] proposed a crack extraction algorithm using gray level correction and adaptive minimum error threshold segmentation that could effectively extract cracks but could not classify or evaluate them. Han *et al.* [6] determined the edges of the cracks and calculated their geometric parameters according to the gray differences between the crack and the background. They used an interactive genetic algorithm to correct the parameters that affect the width of the crack. This algorithm achieved high accuracy but required intensive calculations and had difficulties processing areas in which the cracks and background gray values were similar. Oh *et al.* [7] proposed an algorithm based on the BP neural network. During crack extraction of, a nonlinear classification algorithm was used to classify and test the cracks. This approach also required large amounts of calculation amount and there were

certain requirements for crack selection. Amitrano *et al.* [8] created a method that combined the skeleton line and chain code information to define and describe the characteristics of cracks, which achieved a relatively high detection accuracy. Zhao *et al.* [9] obtained the mechanical equidistant horizontal line on the image on the parametric surface and detected cracks based on the changes of the horizontal force line. This algorithm was based on a simple principle and was not easily affected by external environmental conditions such as stains. However, it required large amounts of calculation and was unable to obtain ideal results for small cracks. Tedeschi and Benedetto [10] used OPENCV library in embedded mobile applications to develop an automatic crack detection system that could detect and provide early warnings for pavement cracks in real time through the mobile network; however, this approach could distinguish only among three main types of cracks and was unable to achieve ideal results for other types of cracks. Cho *et al.* [11] and Zhao *et al.* [12] performed a detailed analysis of the influence of external conditions such as illumination, shooting distance and image definition on crack identification and proposed a plan for improvement. Li *et al.* [13] set up a high-precision image acquisition system and combined the Canny edge detection algorithm and support vector machine to achieve crack identification detection. This algorithm had a good ability to extract cracks with obvious contours, but had difficulty with fine cracks, Wang *et al.* [14] used a multiscale linear filtering approach based on the Hessian matrix to enhance the crack area and then determined the threshold interval according to the maximum entropy of the image histogram to obtain the crack binarization segmentation result. This method achieved a complete and accurate segmentation result, but was based on a relatively complex principle and required large amounts of computation. Peng and Zou [15] used an ant colony algorithm to extract and identify crack images, which achieved ideal results for noisy crack images. Wang and Qi [16] first extracted crack characteristics and then used a support vector machine (SVM) classifier to distinguish the crack images. This approach was both highly accurate and achieved real-time performance. Merazimeksen *et al.* [17] was the first to use the characteristics of crack directivity to distinguish linear and reticulate cracks. They further divided the types of cracks based on density distribution differences. This approach achieved better classification results, but required high-quality crack images and complex calculations.

Due to the unique geographical conditions and complex structures of civil engineering structures, the existing algorithms have difficulties obtaining ideal results when extracting and identifying structural surface cracks. In this study, the adaptive nonlinear grayscale transformation and the OTSU threshold segmentation algorithm to divide the cracks; then, it extracts the number of bifurcation points in the crack skeleton line, the X- and Y-direction peak ratios of a gray projection histogram, the interval ratio of crack distribution, the mean square deviation ratio of gray projection histogram and other crack characteristics. Finally, the classification model uses an SVM algorithm whose optimal kernel parameters are selected by cross validation. The extracted classification features are used as the input, and the model outputs the crack category. This approach is better at extracting and classifying crack images. The steps of Algorithm just as figure 1 shows.

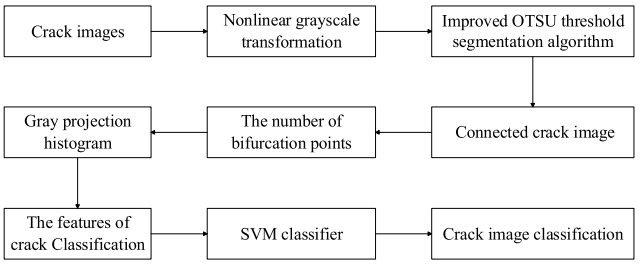

FIGURE 1. Flow chart of the algorithm.

The remaining parts of this paper are as follows: section II introduces the crack segmentation and extraction method on the basis of the gray image features. Section III mainly explains the principles and various characteristics of fracture classification. In section IV, this paper carries out the crack classification experiment by the support vector machine classifier and finds the results of the experiment. Section V is a summary of this paper.

II. CRACK CONTOUR EXTRACTION BASED ON IMAGE GRAYSCALE TRANSFORMATION

A. IMAGE NONLINEAR GRAYSCALE TRANSFORMATION

Crack images often have small color saturation, low contrast and complex backgrounds [18], which makes it difficult to achieve ideal results using traditional threshold segmentation algorithms. In a crack image, the crack, which is a fracture in the ocean engineering structure, is the part with the lowest gray value in the whole image, and the gray values of images with other backgrounds are higher than those of a crack image. Therefore, the nonlinear grayscale transformation is used in this paper to pretreat a crack image in combination with the features of that crack image.

Assuming that the grayscale range of pixels f in the original image is $[a, b]$ and that the grayscale range of pixel g after grayscale transformation is $[a', b']$, the relation between grayscale f and grayscale g is as follows:

$$g = \begin{cases} a' & 0 \le f < a \\ a' + \dfrac{a' - b'}{a^t - b^t}\left(x^t - a^t\right) & a \le f < b \\ b' & b \le f \le f_{\max} \end{cases} \tag{1}$$

In Formula (1), after the linear transformation, the pixels in the original image with a grayscale value less than a will be assigned to a', and the pixels greater than b will be assigned to b'. Finally, the grayscale values of pixels between a and b will be projected to the interval between a and b; when $b' - a' \ge b - a$, this linear change causes the grayscale values of pixels

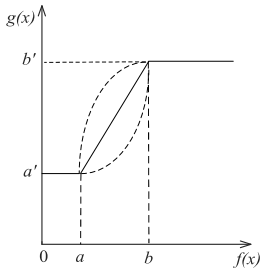

FIGURE 2. Nonlinear grayscale transformation diagram.

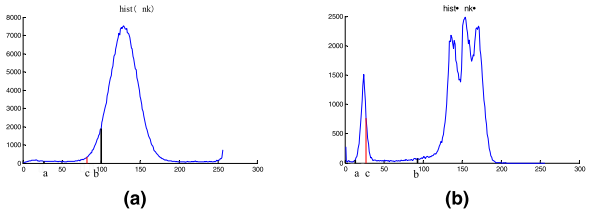

FIGURE 3. Gray histograms of different cracks. Gray histogram of cracks with simple background. (b) Gray histogram of cracks with complex background.

in the interval $[a, b]$ in the original image to become greater, as shown in Fig. 2.

Fig. 2 shows a nonlinear grayscale transformation diagram when the power value t is set to different values. The top dotted line represents the grayscale transformation relation when t is less than 1. The middle solid line is the grayscale linear transformation relation when t is equal to 1, and the lower dotted line represents the grayscale transformation relation when t is greater than 1. To achieve crack image segmentation, we first need to enlarge the grayscale value between the crack and the background pixels: because the crack is in the lowest part of the grayscale value in the image, the purpose of the grayscale transformation is to stretch the grayscale value in that region; therefore, we should choose a grayscale transformation curve where the power value t is less than 1. After determining the grayscale transformation relation, to achieve high-accuracy automatic detection, we need to confirm the transformation interval and the function power value t.

In different images, the ratio of cracks to backgrounds is not the same. Therefore, adopting a fixed threshold for a and b makes it difficult to achieve ideal results in all images [19]. This paper addresses this problem. By analyzing a large number of crack images, we found that the proportion of cracks in images ranges from approximately 2% to 5%: only in a small fraction of crack images does this proportion exceed 5%, and the proportions of other pixels with background grayscale values similar to cracks in crack images ranges from is approximately 5% to 20%, Therefore, we chose the adaptive thresholds a and b to perform the linear grayscale transformation by considering this characteristic of crack images. We set a and b to 0 and 255, respectively, where a represents the upper limit of the grayscale value of the crack region. Therefore, we select the grayscale values of 5% of the pixels with the minimum grayscale values. Here, b represents the lower limit of the grayscale values of pixels whose grayscale values are similar to those in the crack region. Therefore, the grayscale values of pixels whose grayscale values comprise 20% of the image are selected. As shown in Formula (2) and Formula (3):

$$\begin{cases} a' = 0 \\ b' = 255 \end{cases} \tag{2}$$

$$\begin{cases} a = e_1 & \sum_{i=0}^{e_1} p(i) = 0.02 \\ b = e_2 & \sum_{i=0}^{e_2} p(i) = 0.2 \end{cases} \tag{3}$$

After determining the transformation interval, we define the size of the power value t in the nonlinear transformation function because the crack is in the part of the image with the lowest grayscale values, and the grayscale values of similar background points are relatively low; consequently, we primarily want to conduct the gray stretch transformation for the pixels with lower grayscale values. Areas with grayscale values that are much higher than those of the cracks require far less processing. As shown in Fig. 2, when the power value t is less than 1, the stretch effect of the grayscale transformation function on the low grayscale value pixels is much higher than the stretch effect on the high grayscale value pixels: the lower the grayscale value is, the more obvious the stretch effect is. Therefore, using this grayscale transformation function quickly separates the crack-containing area from the background area. The gray characteristics of the image are combined to adaptively select the function power.

We select two crack images, obtain the gray histograms for them, and mark the ranges of the adaptive grayscale transformation areas as shown in Fig. 3.

Two gray histograms of crack images with different background complexities are shown in Fig. 3, where $[a, b]$ represents the pixel interval of the grayscale transformation, and c represents the mean grayscale value in the interval $[a, b]$. In these two gray histograms, the gray distribution of the region in Fig. 3 (a) is more uniform, there are fewer pixels whose grayscale values are similar to those of the crack, and the mean grayscale value c is close to the high threshold b. In addition, the grayscale transformation interval $[a, b]$ is wide. Therefore, a larger function power t can be used to process this image, and the original feature information of the image can be preserved better. In contrast, Fig. 3 (b) shows a peak near the crack area, which indicates that a large number of background pixels are similar to the crack pixels in terms of their grayscale values. In Fig. 3 (b), the mean value c is closer to the low threshold a, and the grayscale transformation interval is relatively narrow. Therefore, a smaller function power t must be used to process it—to widen the gray difference between the crack and the background. Therefore, we define

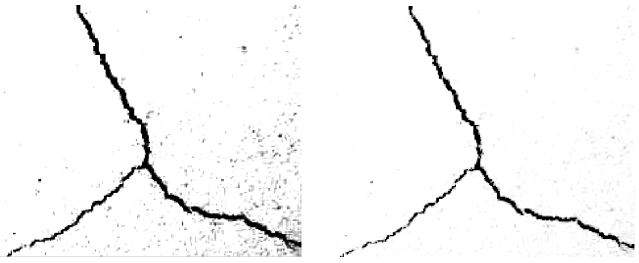

FIGURE 4. Comparison of grayscale transformation effects. (a) Results obtained from linear grayscale transformation. (b) Results obtained from nonlinear grayscale transformation.

the power value t of the nonlinear grayscale transformation function as follows:

$$c = e_1 \sum_{i=a}^{e_1} p(i) = \frac{1}{2} \sum_{i=a}^{b} p(i) \tag{4}$$

$$t = \left(\frac{b-a}{255}\right) \times \frac{2c}{(a+b)} = \frac{2c(b-a)}{255(a+b)}. \tag{5}$$

From these formulae it can be seen that the narrower the transformation interval $[a, b]$ is, the smaller the mean grayscale value c is, the smaller the function power t is, the greater the gray change in the low grayscale value region is, and the greater the gray difference is between the crack area and the background area after transformation. The grayscale value of the crack pixels are preserved in the transformation, while the grayscale values of pixels similar to the crack are stretched, enabling us to process the crack better. A comparison between linear and nonlinear transformation approaches is shown in Fig. 4.

B. IMPROVED OTSU THRESHOLD SEGMENTATION ALGORITHM

After the grayscale transformation of the crack image, the crack can be extracted effectively. In this case, the characteristics of the crack image are combined, and the improved OTSU is used to address it.

The OTSU algorithm [20], which uses a maximum between-class variance method, can use the gray features of an image to divide it into two categories: background and target, thus allowing crack segmentation and extraction. In a grayscale image with a size of $M * N$, assuming that it has L different grayscale levels and the number of pixels in the i^{th} gray level is n_i, the following relationship exists for the entire image:

$$MN = n_0 + n_1 + n_3 + n_4 \cdots + n_{L-1}. \tag{6}$$

In the image, the gray level of the pixels varies from 0 to $L-1$. We first select a level H to divide the gray level into two classes, C_1 and C_2, where C_1 consists of the pixels with grayscale values from 0 to H, and C_2 consists of the pixels with grayscale values from H to L-1. The probabilities at which an image pixel will be assigned to C_1 or C_2 are obtained using the following formula:

$$P_1(C_1) = \frac{1}{M \times N} \sum_{f(i,j) \in C_1} 1 \tag{7}$$

$$P_2(C_2) = 1 - P_1(C_1). \tag{8}$$

The mean gray values of the pixels in parts C_1 and C_2 are represented by m_1 and m_2, respectively:

$$m_1(h) = \sum_{i=0}^{h} iP(i/C_1) = \frac{1}{P_1(h)} \sum_{i=0}^{h} iP_i \tag{9}$$

$$m_2(h) = \sum_{i=h+1}^{l-1} iP(i/C_2) = \frac{1}{P_2(h)} \sum_{i=h+1}^{l-1} iP_i. \tag{10}$$

Based on the above formula, the calculation method for the between-class variance can be written as follows:

$$\begin{aligned} \sigma_B^2 &= p_1(h)\left[m_1(h) - m_g\right]^2 + P_2(h)\left[m_2(h) - m_g\right]^2 \\ &= P_1(h) P_2(h) \left[m_1(h) - m_2(h)\right]^2 \\ &= \frac{\left[m_g P_1(h) - m(h)\right]^2}{P_1(h)\left[1 - p_1(h)\right]} \end{aligned} \tag{11}$$

$m(h)$ means the grayscale superposition value of a pixel from 0 to H and m_g means the mean grayscale value across the entire image.

In the OTSU algorithm, the threshold with the maximum between-class variance is the threshold that will have the best results when segmenting the image background and edges. Using this threshold to process the image obtains the image after segmentation [21]. The classical OTSU algorithm achieves good results in most cases, but in areas where the grayscale value of image changes greatly (such as those with crack edges, etc.), the classical OTSU threshold may cause some errors and fracture phenomena. In this regard, the threshold selection for the OTSU algorithm is improved based on the characteristics, skeleton line and gray mean square error of crack images; the steps are as follows.

1) First, the classical OTSU algorithm is used to detect the image and obtain the global threshold T_1. The calculation is shown in Formula 11.
2) Next, a 7×7 window is used to traverse the image, and the gray mean square deviation D_1 is calculated for the pixels inside each template position.
3) When the global threshold T_1 is greater than the gray mean square variance D_1, T_1 will be used as the segmentation threshold. When the global threshold T_1 is less than the gray mean square variance D_1, the maximum between-class variance of the pixels in the template is recalculated to obtain the template threshold T_2.Thresholds T_1 and T_2 are used to process their respective regions to obtain the threshold segmentation results.
4) The segmentation results is properly expanded, corroded and smoothed to obtain The skeleton line of the crack

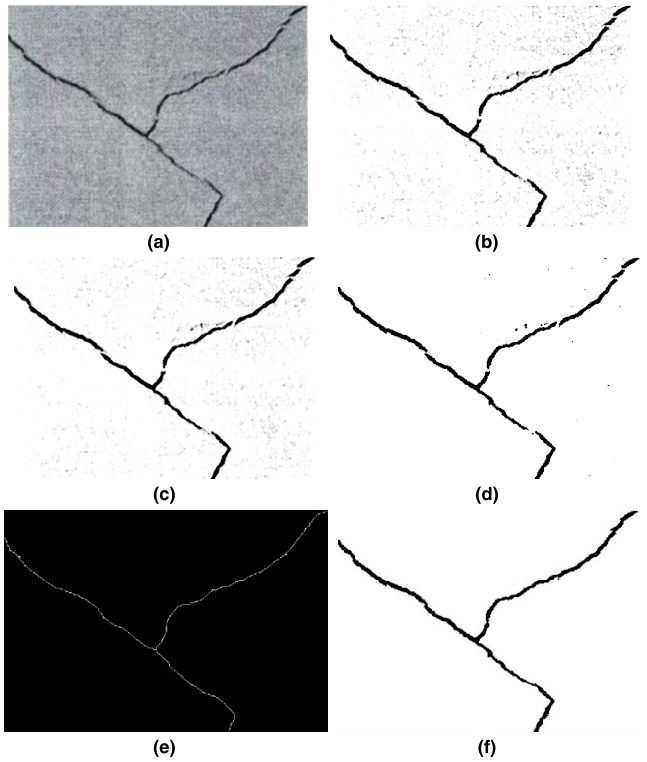

FIGURE 5. Comparison of the detection results of OTSU algorithms before and after improvement. (a) Original crack diagram. (b) nonlinear grayscale transformation. (c) Detection image of the classical OTSU algorithm. (d) Detection image of the improved OTSU algorithm. (e) Single-pixel crack skeleton. (f) Connected crack image.

5) At the fracture point P of the crack, a search is performed along the direction of the skeleton line, and cracks are connected along the skeleton line direction when crack blocks no more than five pixels away from point P are found.
6) A crack boundary point is a point where the grayscale value is mutated more than that of non-crack pixels. Therefore, when we connect, we should select the boundary using this feature and fill in the pixels in the middle of the crack. Finally, we obtain the crack image after the filling process is complete.

To verify the effectiveness of the improved threshold segmentation algorithm in this paper, a transverse crack image is selected and processed. The result in Fig. 5 shows that—compared with the classical algorithm—the edge of the crack image obtained by the improved algorithm segmentation is clearer and more integrated, the errors resulting from the extraction of background pixels are also greatly reduced.

III. RESEARCH ON CLASSIFICATION TECHNOLOGY FOR CONCRETE CRACKS

The concrete structures of civil engineering, under influences from their harsh external environments, easily acquire a variety of cracks on their surfaces. Some of these are linear cracks, such as transverse and vertical cracks, and they may be reflective cracks or new cracks. The damage different types of cracks cause to structures also differs. In this section, we first distinguish linear cracks from reticulate cracks using the bifurcation point of the skeleton line and then make a specific distinction between different types of linear cracks based on a projection of the crack pixels and the variance in the projection.

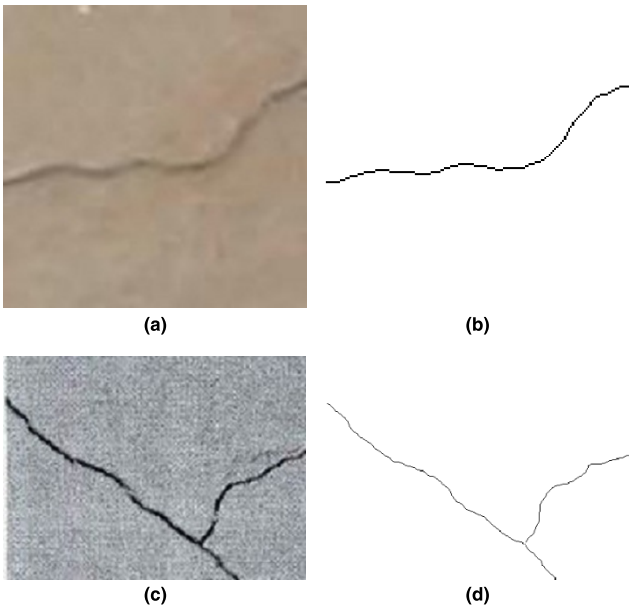

FIGURE 6. Skeleton lines of different types of cracks. (a)Original diagram of a linear crack. (b) Skeleton line of the linear crack. (c)Original diagram of a reticulate crack. (d) Skeleton line of the reticulate crack.

A. CRACK CLASSIFICATION OF BIFURCATION POINTS BASED ON CRACK SKELETON LINE

The skeleton line of a crack is a single-pixel line obtained by the morphological crack operation. The skeleton line preserves a large number of geometric crack characteristics [22], [23]. For example, the direction and trend of the skeleton line accurately reflect the direction and trend of a crack, and its morphological information is almost identical to that of the crack, as shown in Fig. 6.

As shown in Fig.6, the skeleton line of a linear crack is a straight line that follows the same direction as the crack, while the skeleton line of a reticulate crack is also a reticular line featuring the same bifurcation in the same directions. Therefore, we can distinguish between linear cracks and nonlinear cracks based on the existence of a bifurcation in the crack skeleton line. The basic steps are as follows.

1) For a crack image, we first use the improved threshold segmentation algorithm based on the image gray characteristics as discussed in the previous section to segment the crack image.
2) Then, we use the morphological operation and the large sphere method to get the skeleton lines from the segmented images.
3) We set the blank matrix $A\ (i, j)$ and $f\ (i, j)$ to the same size as the crack image and set the areas in the matrix

that have the same location as the crack to 1 and the rest to 0. A left-to-right traversal method is used to traverse the cracks and count the number of its adjacent points. When the number of adjacent points is 2, it is the common crack point. When there are 3 or more, it is a bifurcation point, the number of bifurcation points is t, and the location of the bifurcation point is marked as $f(i,j)$.

$$\begin{cases} \sum_{x\in(i-1,i+1)} \sum_{y\in(j-1,j+1)} A(i,j) \geq 3 \quad f(i,j) = 1 \\ \sum_{x\in(i-1,i+1)} \sum_{y\in(j-1,j+1)} A(i,j) \leq 2 \quad f(i,j) = 0 \end{cases} \tag{12}$$

4) By counting the number of points with a value of 1 in the matrix $A(i,j)$, the total length l of the crack can be obtained, and the length $l(i,j)$ of each bifurcation can be obtained by counting the number of points with the value of 1 after each bifurcation point $f(i,j)$.
5) We can distinguish the type of crack by the number of bifurcation points and the bifurcation length. Considering the inherent characteristics of a crack, we can ignore small burrs and do not consider them for bifurcation. We set a length threshold N for a bifurcation; when a bifurcation length is below N, we consider the bifurcation to be invalid and the bifurcation point is also considered invalid, as shown in Formula 13:

$$\begin{cases} l(i,j) \leq N \quad f(i,j) = 0 \\ l(i,j) \geq N \quad f(i,j) = 1 \end{cases} \tag{13}$$

6) Finally, after obtaining all the non-zero bifurcation points combined with the sum of the effective bifurcation points, we can distinguish the linearity of cracks as shown in the following formula:

$$K = \sum_{(i,j)\in(m,n)} f(i,j) \tag{14}$$

$$\begin{cases} K \geq 1 \quad nonlinear \\ K = 0 \quad linear \end{cases} \tag{15}$$

Based on Formula 15, when the sum of the effective bifurcation points is greater than 1, we can consider the crack to be a reticulate crack, and when the sum of the effective bifurcation points is zero, we consider the crack to be a linear crack.

B. LINEAR CRACK CLASSIFICATION BASED ON GRAY PROJECTION AND MEAN SQUARE ERROR

After differentiating the linearity of the crack, we need to further distinguish the linear crack. Linear cracks are most common form and—based on their direction—can be divided into three types: transverse, vertical and inclined cracks, as shown in Fig. 7.

To distinguish effectively linear cracks, we first analyze the crack images. Transverse cracks have pixels mainly distributed along a row or a few rows, while other areas contain relatively few crack pixels. For vertical cracks, the pixels

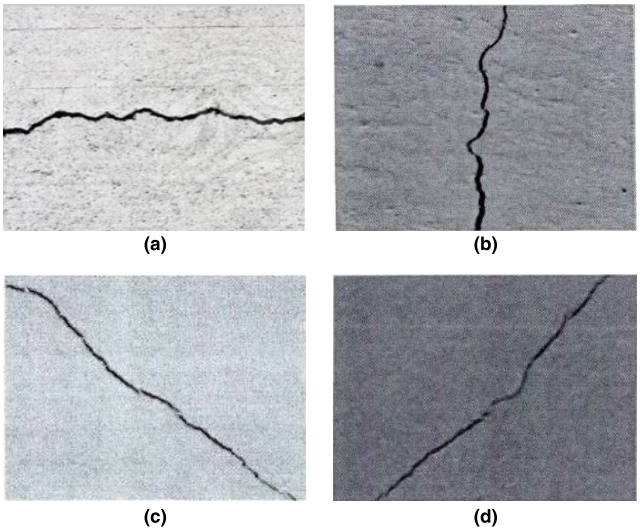

FIGURE 7. Classification of crack images. (a) Transverse crack. (b) Vertical crack. (c) Inclined crack. (d) Inclined crack.

are mainly concentrated in a column or a few columns, and crack pixels in other regions are sparse. For inclined cracks, the pixels are relatively evenly distributed among the rows and columns across a wide range. Therefore, we combine the distinct characteristics of the different directions of the linear crack distribution area and distinguish them based on a gray projection.

For a binarized crack image with a size of $M \times N$, gray projection is carried out in the x-axis and y-axis directions to obtain a gray histogram of the projection as shown in Formulas 16 and 17:

$$V[j] = \sum_{i=1}^{M} Crack(i,j), j = 1, 2, 3 \cdots N \tag{16}$$

$$H[i] = \sum_{j=1}^{N} Crack(i,j), i = 1, 2, 3 \cdots M \tag{17}$$

where $H[i]$ is the horizontal projection histogram obtained from the projection of the image to the y-axis, and $V[j]$ is the vertical projection histogram obtained from the projection of the image to the x-axis. To explain and demonstrate the gray projection results in different directions, we selected crack images in three different directions for simulation processing, and the results are compared and explained. The transverse crack simulation results are shown in Fig. 8.

Fig. 8 shows the result of gray projection for a transverse crack to the x- and y-axes. As shown, for a transverse crack image, the projection histogram to the y-axis will have a large peak. The projection to the x-axis, that is, the histogram of the vertical projection image has smaller crests and the projection distribution is relatively uniform. To further analyze and explain the crack projection algorithm, we select a vertical crack image from a concrete structure for processing. The results are shown in Fig. 9.

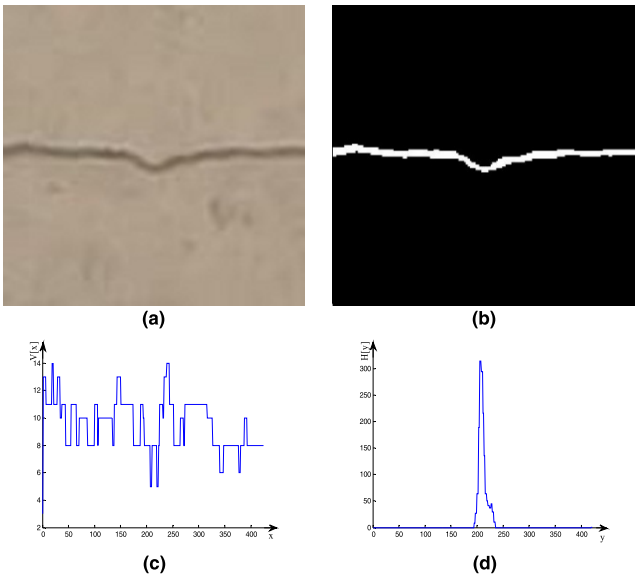

FIGURE 8. Gray projection of transverse cracks. (a) Original diagram of transverse crack. (b) Threshold segmentation results. (c) Projection histogram to the x-axis. (d) Projection histogram to the y-axis.

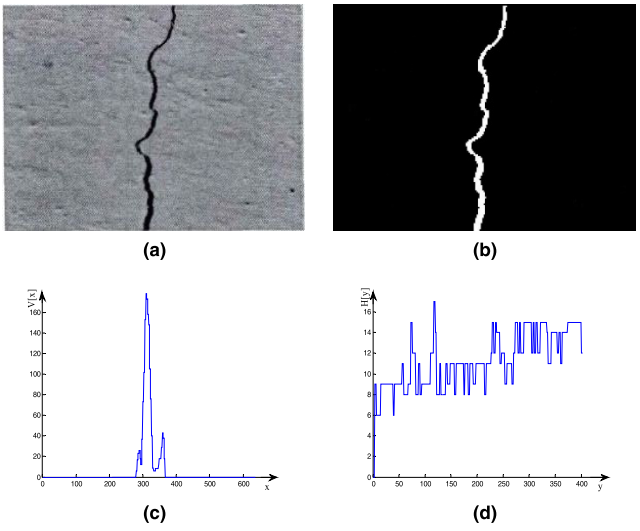

FIGURE 9. Gray projection of vertical cracks. (a) Original diagram of vertical crack. (b) Threshold segmentation results. (c) Projection histogram to the x-axis. (d) Projection histogram to the y-axis.

As shown in Fig. 9, for a vertical crack image, the projection gray histogram to the y-axis will have smaller crests and an even distribution, while the vertical projection gray histogram to the x-axis will have a large peak. The projection distribution is also concentrated. Finally, using an inclined crack image for processing is shown in Fig. 10.

As shown in Fig. 10, the projection gray histograms of an inclined crack to both the x- and y-axes have moderate crests and the projection distribution is uniform. Therefore, we can make a preliminary distinction between fracture types based on the histograms of projection from a crack image to the coordinate axes.

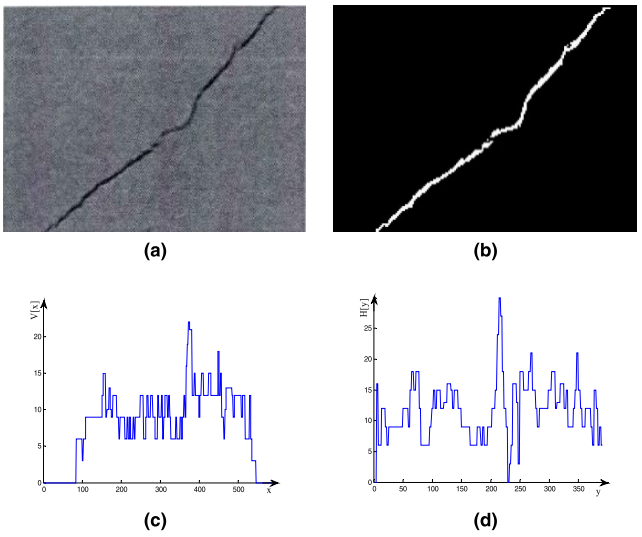

FIGURE 10. Gray projection of inclined cracks. (a) Original diagram of inclined crack. (b) Threshold segmentation results. (c) Projection histogram to the x-axis. (d) Projection histogram to the y-axis.

To further distinguish linear crack types, we further process and analyze the projection histogram of the crack image. First, the distribution range Δx and Δy of the projection histogram on the x-axis and the y-axis is obtained. When the image is a transverse crack, the distribution range Δx of the projection histogram on the x-axis will be far less than the distribution range Δy on the y-axis. Conversely, when the crack is vertical, the distribution range Δy on the y-axis will be much smaller than the distribution range Δx on the x-axis. Finally, the histogram distribution range of an inclined crack image will basically be similar on both pixel axes. Second, we obtain the mean square error for the projection histogram of the crack, set the variance in the horizontal direction to σ_H and the variance in the vertical direction to σ_v. A transverse crack image will have a horizontal variance far greater than its vertical variance, and a vertical crack image will have a vertical variance far greater than its horizontal variance. For an inclined crack image, the variance in both the horizontal and vertical directions will be similar. Therefore, using these characteristics of crack gray projection histograms, we propose a new automatic differentiation method for linear cracks.

1) A linear crack image is first extracted by the threshold segmentation algorithm; then, binarization is conducted to obtain the binarized crack image.
2) The projection transformations on the x- and y-axes are conducted on the binarized crack images, and the projection gray histograms on the x- and y-axes are obtained. The peak values $V_{\max}$ and $H_{\max}$ of the x- and y-axis histograms are obtained, respectively. Finally, the distribution ranges of Δx and Δy values of the projection histograms on the x-axis and the y-axis are calculated as shown in Formula 18:

$$\begin{cases} \Delta x = x_{\max} - x_{\min} \\ \Delta y = y_{\max} - y_{\min} \end{cases} \tag{18}$$

3) The ratios of the peak values and the distribution ranges of the projection histograms in the axes of the crack coordinates are calculated to obtain the peak ratio of K and the distribution range S of the crack projection histograms, as shown in the following formula:

$$K = \frac{V_{\max}}{H_{\max}} \tag{19}$$

$$S = \frac{\Delta y}{\Delta x}. \tag{20}$$

4) The ratio of the mean square error between the projection gray histogram of crack image and that of the x- and y-axes is calculated as shown in Formulas 21–23:

$$\sigma_v = \sqrt{\frac{1}{N}\sum_{i=1}^{N}(V[i]-\mu)^2} \tag{21}$$

$$\sigma_H = \sqrt{\frac{1}{M}\sum_{j=1}^{M}(H[i]-\mu)^2} \tag{22}$$

$$T = \frac{\sigma_H}{\sigma_V} \tag{23}$$

5) The high and low thresholds of the peak ratio of the gray projection histogram of the cracks are assigned to a_1 and a_2, respectively. The high and low thresholds of the distribution range ratio of the histogram on the two axes are assigned to b_1 and b_2, respectively. The high and low thresholds of the histogram mean square error ratio are assigned to c_1 and c_2, respectively. By comparing these three parameters, the linear crack type is distinguished as shown in Formula 24:

$$f = \begin{cases} 1 & 0 \le K \le a_1 \quad 0 \le S \le b_1 \quad 0 \le T \le c_1 \\ 2 & K \ge a_2 \quad S \ge b_2 \quad T \ge c_2 \\ 3 & others \end{cases} \tag{24}$$

In Formula 24, when the f value of the type function of the crack is 1, the crack direction is transverse; when the f value of the type function of the crack is 2, the crack direction is vertical, when the f value of the type function of the crack is 3, the crack direction is inclined.

To further verify and explain the proposed method and formula, we selected 20 transverse, 20 vertical and 20 inclined cracks to obtain the peak ratio K of the projection histogram, the distribution range S, and the mean square error, as shown in Fig. 11.

As shown in Fig. 11, compared with other types of cracks, the peak ratio K, the distribution range S, and the mean square error ratio of the projection histogram of transverse cracks are the smallest. The peak ratio, the distribution range ratio, and the mean square error ratio of the projection histogram of vertical cracks are the largest, and for inclined cracks, the ratio values are between the other two. In addition, the ratios of different types of cracks are very different; therefore, we can distinguish linear crack types quickly and accurately based on the ratios of the parameters of the crack projection histogram.

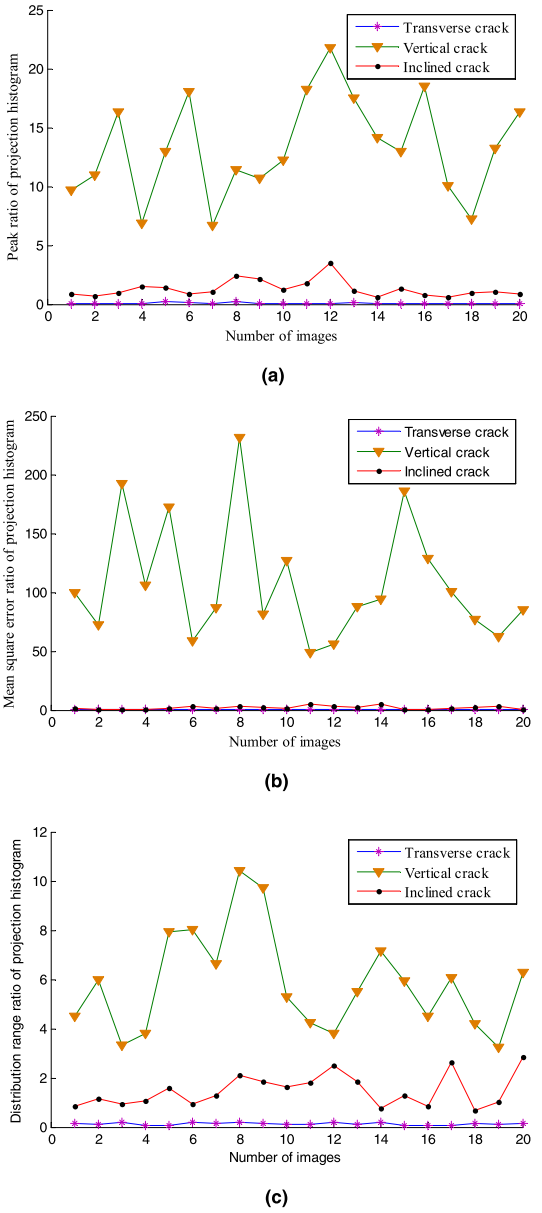

FIGURE 11. Comparison of the parameters of the projection histograms of different types of cracks. (a) Peak ratio of crack projection histogram. (b) Distribution range ratio of crack projection histogram. (c) Mean square error ratio of crack projection histogram.

To distinguish the crack types quickly and accurately, we built an SVM classifier based on the various properties of gray crack projection histograms.

IV. SVM CLASSIFIER

A. SVM PRINCIPLES

The SVM is a supervised learning method that has been widely applied to statistical classifications, regression analysis and so on [24]. The main idea of the SVM is to establish a decision surface through continuous training and maximizing the distance between the samples to be classified. Therefore, the classification problem can be converted to one

of obtaining maxima and minima to make the classification process more accurate.

In SVM algorithms, the two most important parameters are the kernel function g and the penalty factor c. Adopting an appropriate penalty factor c can solve the problem of over-fitting that SVMs are subject to when there are few discrete points. The kernel function reflects the degree of correlation between the support vectors. Therefore, to construct a good SVM classifier, we first used a grid search cross-validation method to optimize the parameters c and g.

B. SVM PARAMETER OPTIMIZATION

1) CROSS VALIDATION

The main purpose of cross validation is to eliminate the deviations caused by random sampling during training [25]. The basic idea is to divide the original samples into two parts: a training set and a test set according to certain rules. First, the training set is used for model training, then, the test set is used to verify the accuracy of the classification model. The commonly used cross-validation methods include repeated random sampling, K-fold cross-validation, and so on. The K-fold cross validation method has high computing efficiency and good accuracy, thus it is widely used. Its basic principle is to divide the original sample into K groups, using one group of samples as the test set and all the other K-1 groups of samples as training sets. Cycling the training sets causes each group to be a test set once. In this way, a total of K models is obtained. Using the mean value of the accuracy rate of the K model test sets as the performance index, the SVM parameter that yields the highest model accuracy is used as the optimization parameter. This approach can greatly improve the stability and generalization ability of the model. During cross-validation process, model accuracy is usually assessed by the minimum mean square error (MMSE). The optimization is carried out in the parameter space, and the parameter that yields the minimum mean square error is selected. The mean square error is:

$$\delta_{MMSE} = \frac{1}{K}\sum_{i=1}^{K}(y_i - \overline{y_i}), \tag{25}$$

Where y_i is the actual value and $\overline{y_i}$ is the estimated value of the cross-validation model.

2) GRID SEARCH

Grid search is an exhaustive method in which the competition space is divided into several parts to calculate and traverse each grid node in the competition space to obtain the optimal solution [26], [27]. Each node participates in the comparison, which makes the selected parameter the global optimal solution and avoids calculation errors caused by artificial specification.

In the SVM algorithm used in this paper, we need to optimize the kernel function g and the penalty factor c. We use the grid method to divide their respective value regions into M and N parts, forming an $M \times N$ grid plane. The MMSE from the estimation model using each parameter combination can be calculated by cross validation. After each node of the grid has been traversed, the parameter combination resulting in the minimum MMSE is selected—that is, the optimal parameter. The specific steps are as follows.

1) Select the parameter initialization range. In this paper, the range of a $= [-5, 5]$, that of b $= [-5, 5]$ and the step size is 0.5. The values for the grid parameter are $c = 2^a$ and $g = 2^b$.
2) Divide the sample. The training data are divided into K subsets. In this paper, K is set to 5. For each set of parameters (c, g) in the grid, a random subset is selected as a test set. The remaining 4 subsets are used as the training sets. Finally, the training set training model is used to predict the test set, and the mean square error values of the test results under this set of parameters are calculated.
3) Obtain the prediction error value. After each of the 5 subsets have been used as a test set, the mean δ_{MMSE} (the error of the mean square error of the 5 sets of predicted results) is taken as the prediction error of the complete set of parameters.
4) Obtain the optimal parameter combination. Change the parameter combination (c, g) and repeat steps 2 and 3, calculating the mean δ_{MMSE} of the mean square error of the grid model under each parameter combination. Finally, select the combination parameter (c, g) that corresponds to the minimum δ_{MMSE} as the optimal parameter combination.

C. SIMULATION AND RESULT ANALYSIS

After selecting and optimizing the parameters, we can build an image classifier based on the trained SVM. In this paper, the SVM type we selected is C-SVC and its kernel function is the RBF kernel [28]. Four characteristics, including the number of bifurcation points of crack skeleton line, are taken as the input sample. The output is the crack type. The training set included 50 images featuring all three crack types. The test set includes 10 images of each type. The classification results are shown in Fig. 12.

Fig. 12(a) shows a contour map for the SVC parameter using classification characteristics such as the crack skeleton line as input, and Fig. 12(b) shows a 3D view of the SVC parameter. Figures 12(a) and 12 (b) show that the penalty factor c obtained by cross validation and grid search is 16, the kernel function g is 32, and the accuracy rate of cross testing is 99.5%. Fig. 12(c) shows that during the course of training, all the crack images can be accurately classified. Thus, the classification accuracy rate of the training set is 100%. As shown in 12 (d), the classification accuracy rate of the test set remains at 100% after using ten images of all crack types for testing. From these results, it can be seen that the selected classification characteristics, including the number of bifurcation points of skeleton lines, can be used to distinguish the different types of crack images effectively and

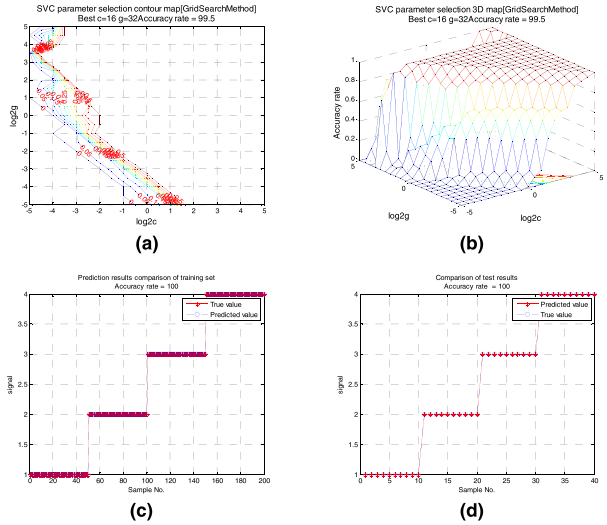

FIGURE 12. Results of crack image classifications. (a) SVC parameter selection contour map. (b) SVC parameter selection 3D view. (c) Comparison of training results. (d) Comparison of test results.

that using these characteristics as input to an SVM classifier achieves ideal results.

V. CONCLUSION

In this paper, problems in national defense engineering structure monitoring—including the large errors that occur during crack image extraction and the related crack classification problem are studied, and a new classification algorithm for concrete crack extraction based on machine vision is proposed. First, the grayscale difference between a crack image and the image background is expanded using the adaptive nonlinear grayscale transformation. An improved OTSU threshold segmentation method is used to extract the cracks, and crack fractures in the extraction results are connected by using the extension direction of the crack skeleton line and the gray features of the crack edge to obtain the complete crack image. Second, crack classification characteristics are extracted such as the number of bifurcation points in the fracture skeleton line, the peak ratio of the gray histogram in the x- and y-axis directions, the projection interval ratios of cracks in the x- and y-axes, the mean square error ratio of the crack gray histogram along the x- and y-axes, and so forth. Finally, the extracted classification characteristics are used as input to train an SVM classifier. Finally, the trained SVM is used to classify crack types. The reported simulation results show that the proposed algorithm can not only extract crack images completely and precisely but also distinguishes and identifies crack types quickly and accurately, resulting in good detection ability.

REFERENCES

[1] Q. Zheng, M. Yang, J. Yang, Q. Zhang, and X. Zhang, "Improvement of generalization ability of deep CNN via implicit regularization in two-stage training process," *IEEE Access*, vol. 6, pp. 15844–15869, Mar. 2018.

[2] S. S. Keerthi and C.-J. Lin, "Asymptotic behaviors of support vector machines with Gaussian kernel," *Neural Comput.*, vol. 15, no. 7, pp. 1667–1689, Jul. 2003.

[3] A. Hänel, C. Schulz, and J. Wirth, "Embedded eigenvalues for an elastic strip with cracks," *Quart. J. Mech. Appl. Math.*, vol. 65, no. 4, pp. 535–554, Nov. 2012.

[4] A. Ayenu-Prah and N. Attoh-Okine, "Evaluating pavement cracks with bidimensional empirical mode decomposition," *J. Adv. Signal Process.*, vol. 20, no. 8, pp. 1–7, Dec. 2008.

[5] J. W. Long, X. J. Shen, and H. P. Chen, "Interactive document images thresholding segmentation algorithm based on image regions," *J. Comput. Res. Develop.*, vol. 49, no. 7, pp. 1420–1431, Jul. 2012.

[6] F. Han, S. Zhao, L. Zhang, and J. Wu, "Survey of strategies for switching off base stations in heterogeneous networks for greener 5G systems," *IEEE Access*, vol. 4, pp. 4959–4973, Aug. 2016.

[7] J.-K. Oh *et al.*, "Bridge inspection robot system with machine vision," *Automat. Construct.*, vol. 18, no. 7, pp. 929–941, Apr. 2009.

[8] D. Amitrano *et al.*, "Feature extraction from multitemporal SAR images using selforganizing map clustering and object-based image analysis," *IEEE J. Sel. Topics Appl. Earth Observ. Remote Sens.*, vol. 11, no. 5, pp. 1556–1570, May 2018.

[9] G. Zhao, T. Wang, and J. Ye, "Surface shape recognition method for crack detection," *J. Electron. Imag.*, vol. 23, no. 3, pp. 1267–1276, May 2014.

[10] A. Tedeschi and F. Benedetto, "A real-time automatic pavement crack and pothole recognition system for mobile Android-based devices," *Adv. Eng. Inform.*, vol. 32, pp. 11–25, Apr. 2017.

[11] H.-W. Cho, H.-J. Yoon, and J.-C. Yoon, "Analysis of crack image recognition characteristics in concrete structures depending on the illumination and image acquisition distance through outdoor experiments," *Sensors*, vol. 16, no. 10, pp. 1646–1667, Oct. 2016.

[12] Y. Zhao, G. Wang, and Y. Liu, "Research of subway tunnel crack recognition algorithm based on image processing," in *Proc. Int. Conf. Elect. Inf. Technol. Rail Transp.*, in Lecture Notes in Electrical Engineering, vol. 287, Feb. 2014, pp. 283–292.

[13] G. Li, X. Zhao, K. Du, F. Ru, and Y. Zhang, "Recognition and evaluation of bridge cracks with modified active contour model and greedy search-based support vector machine," *Automat. Construct.*, vol. 78, pp. 51–61, Jun. 2017.

[14] H. Wang, Y. Zou, Y. Cai, Y. Cheng, and J. Wang, "Crack segmentation in CT image sequences using Hessian matrix and entropy," *Chin. J. Sci. Instrum.*, vol. 37, no. 8, pp. 1800–1807, Aug. 2016.

[15] C. Peng and C. C. Zou, "Automatic extraction method for imaging logs crack based on improved ant colony algorithm," *Comput. Eng.*, vol. 41, no. 8, pp. 196–201, May 2015.

[16] R. Wang and T. Qi, "Study on crack characteristics based on machine vision detection," *China Civil Eng. J.*, vol. 49, no. 7, pp. 123–128, Jul. 2016.

[17] T. Merazi-Meksen, M. Boudraa, and B. Boudraa, "Mathematical morphology for TOFD image analysis and automatic crack detection," *Ultrasonics*, vol. 54, no. 6, pp. 1642–1648, Aug. 2014.

[18] X. Tong, J. Guo, Y. Ling, and Z. Yin, "A new image-based method for concrete bridge bottom crack detection," in *Proc. Int. Conf. Image Anal. Signal Process.*, 2011, pp. 568–571.

[19] A. Zomet, A. Levin, S. Peleg, and Y. Weiss, "Seamless image stitching by minimizing false edges," *IEEE Trans. Image Process.*, vol. 15, no. 4, pp. 969–977, Apr. 2006.

[20] N. Otsu, "A threshold selection method from gray-level histograms," *IEEE Trans. Syst., Man, Cybern.*, vol. SMC-9, no. 1, pp. 62–66, Jan. 1979.

[21] Z. Zhu, S. German, and I. Brilakis, "Visual retrieval of concrete crack properties for automated post-earthquake structural safety evaluation," *Automat. Construct.*, vol. 20, no. 7, pp. 874–883, Nov. 2011.

[22] C. Ge, Z. Sun, N. Wang, K. Xu, and J. Wu, "Energy management in cross-domain content delivery networks: A theoretical perspective," *IEEE Trans. Netw. Service Manage.*, vol. 11, no. 3, pp. 264–277, Sep. 2014.

[23] L. Wang, D. Wang, and C. Hao, "Intelligent CFAR detector based on support vector machine," *IEEE Access*, vol. 5, pp. 26965–26972, Nov. 2017.

[24] K. Cui, W.-H. Yang, and H. Gou, "Experimental research and finite element analysis on the dynamic characteristics of concrete steel bridges with multi-cracks," *J. Vibroeng.*, vol. 19, no. 6, pp. 4198–4209, Oct. 2017.

[25] S. Maldonado, J. López, and M. Carrasco, "A second-order cone programming formulation for twin support vector machines," *Appl. Intell.*, vol. 45, no. 2, pp. 265–276, Sep. 2016.

[26] X.-X. Wen, X.-R. Meng, X.-L. Liang, and Q.-Y. Kang, "Centroid normal direct support vector machine," *Neural Process. Lett.*, vol. 45, no. 2, pp. 563–575, Apr. 2017.

[27] H. Hu and J. Wu, "New constructions of codebooks nearly meeting the Welch bound with equality," *IEEE Trans. Inf. Theory*, vol. 60, no. 2, pp. 1348–1355, Feb. 2014.
[28] K. Cui and X. Qin, "Virtual reality research of the dynamic characteristics of soft soil under metro vibration loads based on BP neural networks," *Neural Comput. Appl.*, vol. 29, no. 5, pp. 1233–1242, Mar. 2018.

SUN LIANG received the B.S. degree in electrical engineering and the automatization specialty from the Nanjing University of Aeronautics and Astronautics, Nanjing, China, in 2012, and the M.Sc. degree in power system and automation from the PLA University of Science and Technology, Nanjing, China, in 2015, where he is currently pursuing the Ph.D. degree with the College of Defense Engineering. His research is focused on image processing, artificial intelligence, machine vision, and relevant fields.

XING JIANCHUN received the B.Sc. and M.Sc. degrees in electric system and automation from the Engineering Institute of Engineering Corps, Nanjing, China, in 1984 and 1987, respectively, and the Ph.D. degree in information system engineering from the PLA University of Science and Technology, Nanjing, China, in 2006.

He is currently a Professor with the PLA University of Science and Technology. His research interests include intelligent control, artificial intelligence, workflow management, and machine vision technology.

ZHANG XUN received the B.S. degree in electrical engineering and the automatization specialty from the Guilin University of Electronic Technology, Guilin, China, in 2010, and the M.Sc. and Ph.D. degrees in power system and automation from the PLA University of Science and Technology, Nanjing, China, in 2013 and 2017, respectively. His research is focused on intelligent control, image processing, artificial intelligence, machine vision, and relevant fields.